Springer

KSME

Journal of Mechanical Science and Technology 26 (7) (2012) 2197~2211
www.springerlink.com/content/1738-494x
DOI 10.1007/s12206-012-0541-1

Tracking control of a three-wheeled omnidirectional mobile manipulator system with disturbance and friction †

Tuan Dinh Viet[1], Phuc Thinh Doan[1], Nguyen Hung[2], Hak Kyeong Kim[1] and Sang Bong Kim[1,*]

[1]*Department of Mechanical and Automotive Eng., College of Eng., Pukyong National University, Busan, 608-739, Korea*
[2]*Faculty of Mechanical – Electrical – Electronic, University of Technology, Hochiminh City, Vietnam*

(Manuscript Received April 25, 2011; Revised October 6, 2011; Accepted January 24, 2012)

Abstract

This paper proposes a tracking control method for a three-wheeled omnidirectional manipulator system (OMMS) with disturbance and friction. The OMMS is separated into two subsystems, a three-wheeled omnidirectional mobile platform (OMP) and a selective compliant articulated robot for assembly (SCARA) type of manipulator. Therefore, two controllers are designed to control the OMP and the manipulator system. Firstly, based on a kinematic modeling of the manipulator, a kinematic controller (KC), combined with an integral sliding mode controller (ISMC), is designed for the end-effector of the manipulator to track a desired trajectory with the desired angular velocity vector of links. Secondly, a differential sliding mode controller (DSMC) based on a dynamic modeling of the OMP with force external disturbances is proposed to obtain control inputs moving the OMP so that the manipulator tracks the desired posture without singularity. The system stability is proven using Lyapunov stability theory. The simulation and experimental results are presented to illustrate the effectiveness of the proposed controllers in the presence of disturbance and friction.

Keywords: Omnidirectional manipulator system (OMMS); Omnidirectional mobile platform (OMP); Integral sliding mode controller (ISMC); Differential sliding mode controller (DSMC)

1. Introduction

An omnidirectional mobile platform with a manipulator is more powerful than a conventional mobile manipulator with regular wheels, especially in life applications such as home-car robot, office robots, nursing robots, medical services and so on. Compared to conventional mobile platforms with two or four regular driving wheels, omnidirectional mobile platforms with three degrees of freedom (DOFs) have an agile ability to move toward any desired direction and to attain the desired orientation simultaneously [1-5].

The omnidirectional mobile manipulator is a typical example of a holonomic mechanical system. However, the omnidirectional mobile manipulator provides some problems from its complicated mechanical structure. For example, it is very difficult to derive the model of an omnidirectional mobile manipulator, especially the dynamic modeling. Furthermore, more redundant actuators also imply that more motors need to be controlled. Therefore, obtaining the modeling and the motion control of an omnidirectional mobile manipulator is sorely needed.

The modeling and the control of the omnidirectional mobile manipulators were presented in Refs. [6, 7]. Watanabe et al. [6] proposed the omnidirectional mobile manipulator without disturbance and surface friction exerted on the omnidirectional mobile platform of the computed torque control and the resolved acceleration control methods. Xu et al. [7] proposed the robust neural network-based sliding mode method for trajectory tracking control of the omnidirectional mobile manipulator with three castor wheels. A robust strategy in controlling the active suspension system using the proportional-integral sliding mode control scheme was presented by Y. M. Sam et al. [18]. H. Zhang et al. [19] proposed the robust $\mathcal{H}_\infty$ PID control such that load and reference disturbances can be attenuated with a prescribed level. N. Hung et al. [10] proposed a control method for the omnidirectional manipulator system to track a desired trajectory with a constant velocity and a desired posture of links. However, they presented only simulation results and did not consider tracking the desired angular velocities of links.

This paper proposes a control method for the omnidirectional manipulator system to track a desired trajectory with a constant velocity at a desired angular velocities and a desired posture of links. The OMMS is separated into two subsystems, a SCARA type of manipulator and a three-wheeled omnidirectional mobile platform. A kinematic controller (KC) based

*Corresponding author. Tel.: +82 51 629 6158, Fax.: +82 51 621 1411
E-mail address: kimsb@pknu.ac.kr
† Recommended by Associate Editor Yang Shi

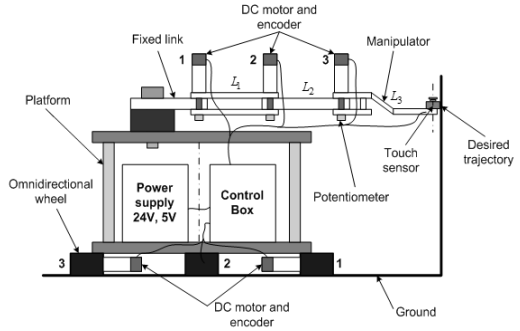

Fig. 1. Configuration of the OMMS.

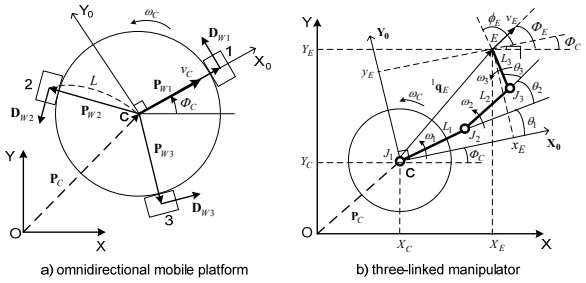

Fig. 2. Configuration for geometric model of the OMMS.

on kinematic modeling of the manipulator is proposed to obtain desired angular velocities of links for the end-effector of the manipulator to track a desired trajectory with a constant velocity. An ISMC based on a dynamic modeling of the manipulator with time-varying external disturbances of links is proposed to obtain control inputs for tracking the real angular velocities to the desired angular velocities of links. A DSMC based on a dynamic modeling of the OMP with force external disturbances due to surface friction and slip phenomenon in wheel axial directions is proposed to obtain control inputs moving the OMP so that the manipulator tracks the desired posture without singularity. Schemes for detecting the tracking errors using a touch sensor and for calculating the posture tracking errors using rotary potentiometers are presented. A control system is developed based on PIC microcontroller. Simulation and experimental results are shown to prove the effectiveness and the applicability of the proposed control method.

2. System description and modeling

2.1 System description

Fig. 1 shows the configuration of an omnidirectional mobile manipulator system (OMMS) used for this paper. It consists of a platform, a SCARA-type manipulator, three omnidirectional wheels, DC motors and encoders, a touch sensor, three potentiometers, power supply and a control system.

Fig. 2 shows the configuration for the geometric model of the OMMS considering two separated subsystems such as an omnidirectional mobile platform (OMP) and a SCARA-type manipulator. The OMP in Fig. 2(a) consists of three omnidirectional wheels equally spaced at 120^o from one another. The three omnidirectional wheels have the same radius denoted by r and are driven by DC motors. L is the distance from the wheel's center to the geometric center C. $\mathbf{P}_{Wi} \in \Re^{2\times1}$ $(i = 1, 2, 3)$ is the position vector of each wheel with respect to the moving coordinate frame CX_0Y_0 attached at point C on the OMP. $\mathbf{D}_{Wi} \in \Re^{2\times1}$ is the drive direction vector of each wheel with respect to the global coordinate frame OXY. $\mathbf{q}_C = [X_C \quad Y_C \quad \Phi_C]^T$ is the posture vector of the OMP in the global coordinate frame. $\mathbf{P}_C = [X_C \quad Y_C]^T$ is defined as the position vector of point C with respect to the global coordinate frame. v_C and ω_C are the linear velocity and the angular velocity of the OMP. The manipulator has three links as shown in Fig. 2(b). $\mathbf{q_E} = [X_E \quad Y_E \quad \Phi_E]^T$ is the posture vector of the end-effector point E with respect to the global coordinate frame. Φ_E is the angle of the linear velocity vector of the end-effector with respect to the global coordinate frame.

To simplify the modeling of the OMMS, the assumptions are given as follows:

(1) Each link is rigid.

(2) Mass of each link is concentrated on the center of each link.

(3) The mass center of the OMMS is coincident with the geometric center C of the OMP.

(4) Kinematic's parameters such as the wheel's radius r, distance L and lengths of links L_1, L_2, L_3 are known exactly.

(5) Moment of inertia of the OMMS is constant during the operation's process.

(6) A torque disturbance vector exerted on the OMMS consists of sinusoidal torque noises exerted on the manipulator, surface friction and slip phenomenon, uncertain dynamic parameters and dynamic interaction between the manipulator and the OMP.

(7) Motion surface is a smooth horizontal plane.

(8) The curvature radius of the desired trajectory is sufficiently larger than the turning radius of the OMMS.

2.2 Modeling of the omnidirectional mobile platform

In this section, kinematic modeling and dynamic modeling of the three-wheeled omnidirectional mobile platform (OMP) are presented [8, 10].

2.2.1 Kinematic modeling of OMP

The rotation matrix $\mathbf{R}(\Phi_C)$ from the moving coordinate frame to the global coordinate frame is given by

$$\mathbf{R}(\Phi_C) = \begin{bmatrix} \cos(\Phi_C) & -\sin(\Phi_C) \\ \sin(\Phi_C) & \cos(\Phi_C) \end{bmatrix} \in \Re^{2\times2}. \quad (1)$$

The position vectors $\mathbf{P}_{W1}, \mathbf{P}_{W2}, \mathbf{P}_{W3} \in \Re^{2\times1}$ of the wheels of the OMP can be obtained as follows:

$$\mathbf{P}_{W1} = L\begin{bmatrix}1\\0\end{bmatrix}, \quad \mathbf{P}_{W2} = \mathbf{R}(\frac{2\pi}{3})\times\mathbf{P}_{W1} = \frac{L}{2}\begin{bmatrix}-1\\\sqrt{3}\end{bmatrix},$$
$$\mathbf{P}_{W3} = \mathbf{R}(\frac{4\pi}{3})\times\mathbf{P}_{W1} = -\frac{L}{2}\begin{bmatrix}1\\\sqrt{3}\end{bmatrix}. \quad (2)$$

The drive direction vectors of the i^{th} wheel $\mathbf{D}_{Wi} \in \Re^{2\times1}$ $(i = 1, 2, 3)$ are calculated as follows:

$$\mathbf{D}_{Wi} = \frac{1}{L}\mathbf{R}(\Phi_C)\times\mathbf{P}_{Wi}, \qquad \mathbf{D}_{W1} = \begin{bmatrix}0\\1\end{bmatrix},$$
$$\mathbf{D}_{W2} = -\frac{1}{2}\begin{bmatrix}\sqrt{3}\\1\end{bmatrix}, \qquad \mathbf{D}_{W3} = \frac{1}{2}\begin{bmatrix}\sqrt{3}\\-1\end{bmatrix}. \quad (3)$$

The angular velocity of the i^{th} wheel ω_i $(i = 1, 2, 3)$ can be expressed as

$$\omega_i = \frac{1}{r}[\dot{\mathbf{P}}_C^T\times\mathbf{R}(\Phi_c)\times\mathbf{D}_{Wi} + \mathbf{P}_{Wi}^T\times\dot{\mathbf{R}}^T(\Phi_c)\times\mathbf{R}(\Phi_c)\times\mathbf{D}_{Wi}]. \quad (4)$$

From Eq. (4), the kinematic equation of a three-wheeled omnidirectional mobile platform can be expressed as follows:

$$\begin{bmatrix}\omega_1\\\omega_2\\\omega_3\end{bmatrix} = \frac{1}{r}\begin{bmatrix}-\sin\Phi_C & \cos\Phi_C & L\\ -\sin(\pi/3-\Phi_C) & -\cos(\pi/3-\Phi_C) & L\\ \sin(\pi/3+\Phi_C) & -\cos(\pi/3+\Phi_C) & L\end{bmatrix}\begin{bmatrix}\dot{X}_C\\\dot{Y}_C\\\dot{\Phi}_C\end{bmatrix}. \quad (5)$$

Eq. (5) can be rewritten as

$$\mathbf{z} = \frac{1}{r}\mathbf{H}^{-1}\times\dot{\mathbf{q}}_\mathbf{C} \quad (6)$$
$$\mathbf{H}^{-1} = \begin{bmatrix}-\sin\Phi_C & \cos\Phi_C & L\\ -\sin(\pi/3-\Phi_C) & -\cos(\pi/3-\Phi_C) & L\\ \sin(\pi/3+\Phi_C) & -\cos(\pi/3+\Phi_C) & L\end{bmatrix}$$

where $\mathbf{z} \equiv [\omega_1 \quad \omega_2 \quad \omega_3]^T$ is the wheel angular velocity vector.

From Eq. (6), a velocity vector of point C on the OMP is reduced into

$$\dot{\mathbf{q}}_\mathbf{C} = r\,\mathbf{H}\,\mathbf{z}. \quad (7)$$

In Fig. 2(a), a velocity vector of the OMP is obtained as

$$\boldsymbol{\varepsilon} \equiv \begin{bmatrix}v_C\\\omega_C\end{bmatrix} = \begin{bmatrix}\cos\Phi_C & \sin\Phi_C & 0\\ 0 & 0 & 1\end{bmatrix}\dot{\mathbf{q}}_\mathbf{C}. \quad (8)$$

2.2.2 Dynamic modeling of OMP

According to Newton's second law of motion, equations of linear and angular momentum balance of the OMP including a force disturbance vector due to surface friction and slip phenomena can be written as follows:

$$\sum_{i=1}^{3}(f_i - f_{Mi})\mathbf{R}(\Phi_C)\times\mathbf{D}_{Wi} - \mathbf{F}_A = m\ddot{\mathbf{P}}_C \quad (9)$$

$$L\sum_{i=1}^{3}(f_i - f_{Mi}) = I\ddot{\Phi}_C \quad (10)$$

$$\mathbf{F}_A = \begin{bmatrix} f_{A1}\cos\Phi_C + f_{A2}\cos(\frac{2\pi}{3}+\Phi_C) + f_{A3}\cos(\frac{4\pi}{3}+\Phi_C)\\ f_{A1}\sin\Phi_C + f_{A2}\sin(\frac{2\pi}{3}+\Phi_C) + f_{A3}\sin(\frac{4\pi}{3}+\Phi_C)\end{bmatrix}$$

where $\mathbf{F_A}$ is a force disturbance vector due to surface friction and slip phenomena in the wheel axial direction, f_{Mi} and f_{Ai} $(i = 1,2,3)$ are the magnitudes of friction forces exerted on the i^{th} wheel in the wheel motion direction and in the wheel axial direction, respectively, $\ddot{\mathbf{P}}_C \in \Re^{2\times1}$ is the linear acceleration vector, $\ddot{\Phi}_C$ is the angular acceleration, f_i $(i = 1, 2, 3)$ is the magnitude of the force exerted on each wheel driven by the i^{th} motor, m is the mass of the OMP, and I is the moment of inertia for the OMMS about its center of gravity of the OMP.

From the dynamic characteristic of the DC motor, the force generated by a wheel attached to a DC motor is described by [8, 10]:

$$f_i = \alpha u_i - \beta v_{Wi} \quad (11)$$

where u_i $(i = 1, 2, 3)$ is the voltage applied to the DC motors, v_{Wi} $(i = 1, 2, 3)$ is the linear velocity of each wheel, α and β are motor characteristic coefficients depending on the parameters of the DC motor that can be obtained from the its catalog or experiment. $\alpha = k_t/(rR_a)$ and $\beta = k_t k_e n/(r^2 R_a)$ are motor characteristic coefficients depending on the parameters of the DC motor , k_e is the back emf coefficient, k_t is the torque coefficient, r is the radius of each wheel, R_a is the armature resistance and n is gear ratio.

From Eqs. (9)-(11), the dynamic equations of OMP can be expressed as

$$\bar{\mathbf{M}}\ddot{\mathbf{q}}_\mathbf{C} + \bar{\mathbf{V}}\dot{\mathbf{q}}_\mathbf{C} = \mathbf{u} - \mathbf{u}_d \quad (12)$$
$$\bar{\mathbf{M}} = \frac{1}{\alpha}\mathbf{H}^\mathbf{T}\mathbf{M} \in \Re^{3\times3}, \quad \bar{\mathbf{V}} = \frac{1}{\alpha}\mathbf{H}^\mathbf{T}\mathbf{V} \in \Re^{3\times3},$$
$$\mathbf{u}_d = \frac{1}{\alpha}\mathbf{H}^T\mathbf{f}_d \in \Re^{3\times1} \quad (13)$$
$$\mathbf{M} = \begin{bmatrix}m & 0 & 0\\ 0 & m & 0\\ 0 & 0 & I\end{bmatrix}, \quad \mathbf{V} = \begin{bmatrix}1.5\beta & 0 & 0\\ 0 & 1.5\beta & 0\\ 0 & 0 & 3\beta L^2\end{bmatrix}$$

where $\mathbf{u} \equiv [u_1 \quad u_2 \quad u_3]^T \in \Re^{3\times1}$ is a voltage input vector applied to the DC motor, $\mathbf{f}_d \equiv [f_{1d} \quad f_{2d} \quad f_{3d}]^T \in \Re^{3\times1}$ is a friction and slip force disturbance vector as follows:

$$f_{1d} = -f_{M1}\sin\Phi_C - f_{M2}\sin(\pi/3-\Phi_C) + f_{M3}\sin(\pi/3+\Phi_C) + f_{A1}\cos\Phi_C + f_{A2}\cos(2\pi/3+\Phi_C) + f_{A3}\cos(4\pi/3+\Phi_C)$$

$$
\begin{aligned}
f_{2d} &= f_{M1}\cos\Phi_C - f_{M2}\cos(\pi/3-\Phi_C) \\
&\quad - f_{M3}\cos(\pi/3+\Phi_C) \\
&\quad + f_{A1}\sin\Phi_C + f_{A2}\sin(2\pi/3+\Phi_C) \\
&\quad + f_{A3}\sin(4\pi/3+\Phi_C) \\
f_{3d} &= L(f_{M1}+f_{M2}+f_{M3}),
\end{aligned} \tag{14}
$$

$$
-\frac{mg}{3}\mu_{M\max} \le f_{Mi} \le \frac{mg}{3}\mu_{M\max}
$$

$$
-\frac{mg}{3}\mu_{A\max} \le f_{Ai} \le \frac{mg}{3}\mu_{A\max}, \quad i=1,2,3
$$

where $\mu_{M\max}$ and $\mu_{A\max}$ are the maximum static friction coefficients in the wheel motion direction and in the wheel axial direction, respectively [9], and g is the acceleration of gravity.

2.3 Modeling of the three-linked manipulator

In this section, kinematic modeling and dynamic modeling of the three-linked manipulator are presented.

2.3.1 Kinematic modeling of manipulator

In Fig. 2(b), the kinematic equation of the end-effector of the manipulator with respect to the global coordinate frame is obtained as follows [10-13]:

$$
\mathbf{V}_E = \mathbf{V}_C + \mathbf{W}_C\ {}^0\mathbf{Rot}_1\ {}^1\mathbf{q}_E + {}^0\mathbf{Rot}_1\ \mathbf{J}\dot{\boldsymbol{\theta}} \tag{15}
$$

$$
\mathbf{V}_E \equiv \dot{\mathbf{q}}_E = \begin{bmatrix} \dot{X}_E \\ \dot{Y}_E \\ \dot{\Phi}_E \end{bmatrix},\ \mathbf{V}_C \equiv \dot{\mathbf{q}}_C = \begin{bmatrix} \dot{X}_C \\ \dot{Y}_C \\ \dot{\Phi}_C \end{bmatrix},\ \mathbf{W}_C \equiv \begin{bmatrix} 0 \\ 0 \\ \dot{\Phi}_C \end{bmatrix},
$$

$$
{}^0\mathbf{Rot}_1 = \begin{bmatrix} \cos\Phi_C & -\sin\Phi_C & 0 \\ \sin\Phi_C & \cos\Phi_C & 0 \\ 0 & 0 & 1 \end{bmatrix},
$$

$$
{}^1\mathbf{q}_E \equiv \begin{bmatrix} x_E \\ y_E \\ \phi_E \end{bmatrix} = \begin{bmatrix} L_1C_1 + L_2C_{12} + L_3C_{123} \\ L_1S_1 + L_2S_{12} + L_3S_{123} \\ \phi_E \end{bmatrix} \tag{16}
$$

$$
\mathbf{J} = \begin{bmatrix} -L_3S_{123} - L_2S_{12} - L_1S_1 & -L_3S_{123} - L_2S_{12} & -L_3S_{123} \\ L_3C_{123} + L_2C_{12} + L_1C_1 & L_3C_{123} + L_2C_{12} & L_3C_{123} \\ 1 & 1 & 1 \end{bmatrix} \tag{17}
$$

where $\mathbf{V}_E$ and $\mathbf{V}_C$ are the velocity vectors of the end-effector and the center point of the OMP with respect to the global coordinate frame, respectively; $\mathbf{W}_C$ is the angular velocity vector of the moving coordinate frame; ${}^0\mathbf{Rot}_1$ is the rotation transform matrix from the moving coordinate frame to the global coordinate frame; ${}^1\mathbf{q}_E$ is the posture vector of the end-effector with respect to the moving coordinate frame; $\mathbf{J}$ is the Jacobian matrix; $\dot{\boldsymbol{\theta}} \equiv \begin{bmatrix} \dot{\theta}_1 & \dot{\theta}_2 & \dot{\theta}_3 \end{bmatrix}^T$ is the angular velocity vector of the revolution joints of the three-linked manipulator; L_1, L_2, L_3 are the lengths of links of the manipulator, and $S_1 \equiv \sin(\theta_1)$, $S_{12} \equiv \sin(\theta_1+\theta_2)$, $S_{123} \equiv \sin(\theta_1+\theta_2+\theta_3)$, $C_{12} \equiv \cos(\theta_1+\theta_2)$, $C_1 \equiv \cos(\theta_1)$, and $C_{123} \equiv \cos(\theta_1+\theta_2+\theta_3)$.

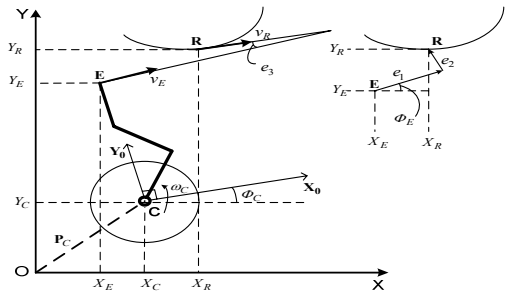

Fig. 3. A tracking error vector $\mathbf{e}_o$ of the manipulator.

2.3.2 Dynamic modeling of manipulator

The dynamic equation of the three-linked manipulator with a time-varying external disturbance vector can be written as [14]

$$
\mathbf{M}_1(\boldsymbol{\theta})\ddot{\boldsymbol{\theta}} + \mathbf{V}_1(\boldsymbol{\theta},\dot{\boldsymbol{\theta}}) + \mathbf{G}_1(\boldsymbol{\theta}) + \boldsymbol{\tau}_{1d} = \boldsymbol{\tau}_M \tag{18}
$$

$$
\mathbf{M}_1(\boldsymbol{\theta}) = \begin{bmatrix} M_{11} & M_{12} & M_{13} \\ M_{21} & M_{22} & M_{23} \\ M_{31} & M_{32} & M_{33} \end{bmatrix},\ \mathbf{V}_1(\boldsymbol{\theta},\dot{\boldsymbol{\theta}}) = \begin{bmatrix} V_{11} \\ V_{21} \\ V_{31} \end{bmatrix},
$$

$$
\mathbf{G}_1(\boldsymbol{\theta}) = \begin{bmatrix} G_{11} \\ G_{21} \\ G_{31} \end{bmatrix},\ \boldsymbol{\tau}_M = \begin{bmatrix} \tau_{M1} \\ \tau_{M2} \\ \tau_{M3} \end{bmatrix},\ \boldsymbol{\tau}_{1d} = \begin{bmatrix} \tau_{1d1} \\ \tau_{1d2} \\ \tau_{1d3} \end{bmatrix}
$$

where $\mathbf{M}_1(\boldsymbol{\theta})$ is the inertia matrix, $\mathbf{V}_1(\boldsymbol{\theta},\dot{\boldsymbol{\theta}})$ is the Centripetal and Coriolis matrix, $\mathbf{G}_1(\boldsymbol{\theta})$ is the gravity vector, $\boldsymbol{\tau}_M$ is the control input torque vector, $\boldsymbol{\tau}_{1d}$ is the time-varying external disturbance vector, and $\boldsymbol{\theta} \equiv [\theta_1 \quad \theta_2 \quad \theta_3]^T$ is a joint angular vector.

The parameters of Eq. (18) are shown in appendix.

3. Controller design

3.1 Controller design of manipulator

For trajectory tracking of the manipulator, a kinematic controller (KC), combined with an integral sliding mode controller (ISMC), is designed for the end-effector of the manipulator to track a desired trajectory with a desired angular velocity vector of links as shown in Fig. 3.

To design the controller, a tracking error vector $\mathbf{e}_o$ between a reference point R and the end-effector point E is defined as follows:

$$
\mathbf{e}_o \equiv \begin{bmatrix} e_1 & e_2 & e_3 \end{bmatrix}^T = \mathbf{A}[\mathbf{q}_R - \mathbf{q}_E] \tag{19}
$$

$$
\mathbf{A} = \begin{bmatrix} \cos\Phi_E & \sin\Phi_E & 0 \\ -\sin\Phi_E & \cos\Phi_E & 0 \\ 0 & 0 & 1 \end{bmatrix},\ \mathbf{q}_R = \begin{bmatrix} X_R \\ Y_R \\ \Phi_R \end{bmatrix}
$$

where $\mathbf{q}_R$ is the posture vector of the reference point which is

moving along a desired trajectory with a constant velocity.

Lyapunov function candidate is defined as follows:

$$\mathbf{V}_o = \frac{1}{2}\mathbf{e}_o^T\mathbf{e}_o . \tag{20}$$

From Eqs. (15), (19) and (20) by Lyapunov stability, the following kinematic control law $\dot{\boldsymbol{\theta}}_d \equiv \begin{bmatrix}\dot{\theta}_{1d} & \dot{\theta}_{2d} & \dot{\theta}_{3d}\end{bmatrix}^T$ for the end-effector of the manipulator to track a desired trajectory is chosen as follows [10-12]:

$$\begin{aligned}\dot{\boldsymbol{\theta}}_d = \mathbf{J}^{-1}\,{}^0\mathbf{Rot}_1^{-1}[\mathbf{A}^{-1}(\dot{\mathbf{A}}\mathbf{A}^{-1}+\mathbf{K})\mathbf{e}_o \\ +\mathbf{V}_R - \mathbf{V}_C - \mathbf{W}_C\,{}^0\mathbf{Rot}_1\,{}^1\mathbf{q}_E]\end{aligned} \tag{21}$$

where $\mathbf{K} = diag(k_1, k_2, k_3)$ is the diagonal positive gain matrix and $\mathbf{V}_R = \dot{\mathbf{q}}_R$. The kinematic control law Eq. (21) exists due to $\mathbf{det(J)} \neq \mathbf{0}$ when link 1 and link 2 are not on the same straight line.

In the following, an ISMC is presented based on the dynamic modeling of the manipulator for making its real angular velocity vector converge to a desired angular velocity vector.

Second, a torque control law $\boldsymbol{\tau}_M$ exerted to links of the manipulator is chosen as

$$\boldsymbol{\tau}_M = \mathbf{M}_1(\boldsymbol{\theta})\ddot{\boldsymbol{\theta}}_d + \mathbf{V}_1(\boldsymbol{\theta},\dot{\boldsymbol{\theta}}) + \mathbf{G}_1(\boldsymbol{\theta}) + \mathbf{M}_1(\boldsymbol{\theta})\boldsymbol{\mu} + \boldsymbol{\tau}_{1d} \tag{22}$$

where $\boldsymbol{\mu} \in \Re^{3\times1}$ is an auxiliary control input vector.

From Eqs. (18) and (22), the following form is obtained

$$\ddot{\boldsymbol{\theta}} - \ddot{\boldsymbol{\theta}}_d = \boldsymbol{\mu} . \tag{23}$$

An angular velocity error vector $\mathbf{e}_v \in \Re^{3\times1}$ is defined as

$$\mathbf{e}_v \equiv [e_{v1} \quad e_{v2} \quad e_{v3}]^T = \dot{\boldsymbol{\theta}} - \dot{\boldsymbol{\theta}}_d \tag{24}$$

where $\dot{\boldsymbol{\theta}}_d$ is a desired angular velocity vector of links of the manipulator.

An integral sliding surface vector $\mathbf{S}_v \equiv \begin{bmatrix}S_{v4} & S_{v5} & S_{v6}\end{bmatrix}^T \in \Re^{3\times1}$ is defined with the angular velocity error vector and its integral term as follows:

$$\mathbf{S}_v = \mathbf{e}_v + \mathbf{K}_v\int \mathbf{e}_v\mathbf{dt} \tag{25}$$

where $\mathbf{K}_v = diag(K_{v4}, K_{v5}, K_{v6})$ is a diagonal positive integral gain matrix.

Third, an auxiliary control input vector $\boldsymbol{\mu}$ for the real angular velocity $\dot{\boldsymbol{\theta}}$ of the manipulator to track the desired angular velocity vector $\dot{\boldsymbol{\theta}}_d$ is designed as follows:

$$\boldsymbol{\mu} = -\mathbf{Q}_v\mathbf{S}_v - \mathbf{P}_v\,\mathbf{sign}(\mathbf{S}_v) - \mathbf{K}_v(\dot{\boldsymbol{\theta}} - \dot{\boldsymbol{\theta}}_d) \tag{26}$$

where the matrices $\mathbf{P}_v = diag(P_{v4}, P_{v5}, P_{v6})$ and $\mathbf{Q}_v = diag(Q_{v4}, Q_{v5}, Q_{v6})$ are diagonal positive definite matrices.

Theorem 3.1: For the kinematic Eq. (6) and the dynamic modeling Eq. (12) of the manipulator with a torque disturbance vector, if the control laws in Eqs. (21), (22) and (26) are applied, both a tracking error vector $\mathbf{e}_o$ and an auxiliary angular velocity error vector $\mathbf{e}_v$ converge to zero asymptotically as $t \to \infty$.

Proof: Lyapunov function candidate is defined as

$$V_1 = V_o + \frac{1}{2}\mathbf{S}_v^T\mathbf{S}_v . \tag{27}$$

The first order derivative of V_1 is derived into

$$\dot{V}_1 = \dot{V}_o + \mathbf{S}_v^T\dot{\mathbf{S}}_v . \tag{28}$$

From Eqs. (15), (19)-(21), the following can be obtained.

$$\begin{aligned}\dot{\mathbf{e}}_o &= \dot{\mathbf{A}}[\mathbf{q}_R - \mathbf{q}_E] + \mathbf{A}[\mathbf{V}_R - \mathbf{V}_E] \\ &= \dot{\mathbf{A}}\mathbf{A}^{-1}\mathbf{e}_o + \mathbf{A}[\mathbf{V}_R - \mathbf{V}_E] \\ &= -\mathbf{K}\mathbf{e}_\mathbf{o}\end{aligned} \tag{29}$$

From Eqs. (23)-(25), the first order derivative of $\mathbf{S}_v$ is given as

$$\begin{aligned}\dot{\mathbf{S}}_v &= \dot{\mathbf{e}}_v + \mathbf{K}_v\mathbf{e}_v = (\ddot{\boldsymbol{\theta}} - \ddot{\boldsymbol{\theta}}_d) + \mathbf{K}_v(\dot{\boldsymbol{\theta}} - \dot{\boldsymbol{\theta}}_d) \\ &= \boldsymbol{\mu} + \mathbf{K}_v(\dot{\boldsymbol{\theta}} - \dot{\boldsymbol{\theta}}_d)\end{aligned} . \tag{30}$$

Substituting Eq. (26) into Eq. (30), the following is obtained as

$$\dot{\mathbf{S}}_v = -\mathbf{Q}_v\mathbf{S}_v - \mathbf{P}_v\,\mathbf{sign}(\mathbf{S}_v) . \tag{31}$$

From Eqs. (3.11) and (3.13), the first order derivative of V_1 is derived into

$$\begin{aligned}\dot{V}_1 &= \mathbf{e}_o^T\dot{\mathbf{e}}_o + \mathbf{S}_v^T\dot{\mathbf{S}}_v = -\mathbf{K}\mathbf{e}_o^\mathbf{2} + \mathbf{S}_v^T\left[-\mathbf{Q}_v\mathbf{S}_v - \mathbf{P}_v\,\mathbf{sign}(\mathbf{S}_v)\right] \\ &= -\mathbf{K}\mathbf{e}_o^\mathbf{2} - \sum_{i=4}^{6}(Q_{vi}S_{vi}^2 + P_{vi}|S_{vi}|) \le 0\end{aligned} . \tag{32}$$

If $Q_{vi} \ge 0$ and $P_{vi} \ge 0$ ($i = 4, 5, 6$), $\dot{V}_1$ is negative under the conditions of Eqs. (20), (21) and (26). By Barbalat's lemma [13], $\mathbf{e}_o \to 0$ and $\mathbf{S}_v \to 0$ as $t \to \infty$. When $\mathbf{S}_v \to 0$, $\mathbf{e}_v = -\mathbf{K}_v\int \mathbf{e}_v dt$ from Eq. (25). So it is clear that $\mathbf{e}_v \to 0$ as $t \to \infty$.

3.2 Differential sliding mode controller (DSMC) design for the OMP

The following shows how to design a differential sliding mode controller (DSMC) based on the dynamic modeling of the OMP to move the manipulator to the desired posture without its singularity.

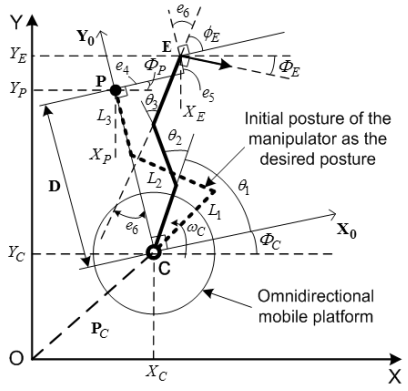

Fig. 4. Posture error vector $\mathbf{e}$ of the manipulator.

The desired posture of the manipulator is chosen with the initial posture of the manipulator as $\theta_{1d} = \pi/4$, $\theta_{2d} = \pi/2$, $\theta_{3d} = -\pi/4$. $\mathbf{q}_P \equiv [X_P, Y_P, \Phi_P]^T$ is a posture vector of the fixed point P as a target point of the end-effector with respect to the global coordinate frame that keeps the desired posture of the manipulator without its singularity. In Fig. 4, the coordinates of the target point P is expressed as follows:

$$X_P = X_C - D\sin\Phi_C\,,\quad Y_P = Y_C + D\cos\Phi_C\,,\quad \Phi_P = \Phi_C \tag{33}$$

where $D = L_1 \sin\left(\frac{\pi}{4}\right) + L_2 \sin\left(\frac{3\pi}{4}\right) + L_3 \sin\left(\frac{\pi}{2}\right)$.

A posture error vector $\mathbf{e} \in \Re^{3\times 1}$ for the OMP is defined as the difference between a target point P and a real point E of the end-effector in Fig. 4.

$$\begin{aligned}\mathbf{e} &\equiv [e_4 \quad e_5 \quad e_6]^T = \mathbf{G}[\mathbf{q}_E - \mathbf{q}_P] \\ &= \mathbf{G}[\mathbf{q}_E - \mathbf{q}_C] + [0 \quad -D \quad 0]^T \\ \mathbf{G} &= \begin{bmatrix} \cos\Phi_C & \sin\Phi_C & 0 \\ -\sin\Phi_C & \cos\Phi_C & 0 \\ 0 & 0 & 1 \end{bmatrix}\end{aligned} \tag{34}$$

The first and second order derivatives of $\mathbf{e}$ yield

$$\dot{\mathbf{e}} = \begin{bmatrix} \dot{e}_4 \\ \dot{e}_5 \\ \dot{e}_6 \end{bmatrix} = \mathbf{G}[\dot{\mathbf{q}}_E - \dot{\mathbf{q}}_C] + [\omega_C(e_5 + D) \quad -\omega_C e_4 \quad 0]^T \tag{35}$$

$$\ddot{\mathbf{e}} = \begin{bmatrix} \ddot{e}_4 \\ \ddot{e}_5 \\ \ddot{e}_6 \end{bmatrix} = \mathbf{G}[\ddot{\mathbf{q}}_E - \ddot{\mathbf{q}}_C] + \begin{bmatrix} \dot{\omega}_C(e_5 + D) + 2\omega_C\dot{e}_5 + \omega_C^2 e_4 \\ -\dot{\omega}_C e_4 - 2\omega_C\dot{e}_4 + \omega_C^2(e_5 + D) \\ 0 \end{bmatrix}. \tag{36}$$

A differential sliding surface vector $\mathbf{S} \equiv [S_4 \quad S_5 \quad S_6]^T$ is defined with the posture error vector and its derivative as follows:

$$\mathbf{S} \equiv \begin{bmatrix} S_4 \\ S_5 \\ S_6 \end{bmatrix} = \begin{bmatrix} \dot{e}_4 + k_4 e_4 \\ \dot{e}_5 + k_5 e_5 \\ \dot{e}_6 + k_6 e_6 \end{bmatrix} \tag{37}$$

where k_4, k_5 and k_6 are positive values.

First, a control input voltage vector $\mathbf{u} \equiv [u_1 \quad u_2 \quad u_3]^T$ for the OMP is defined as follows:

$$\mathbf{u} = \bar{\mathbf{M}}\ddot{\mathbf{q}}_E + \bar{\mathbf{V}}\dot{\mathbf{q}}_C + \bar{\mathbf{M}}\boldsymbol{\eta} + \mathbf{u}_d \tag{38}$$

where $\ddot{\mathbf{q}}_E \in \Re^{3\times 1}$ is a reference acceleration vector and $\boldsymbol{\eta} \in \Re^{3\times 1}$ is an auxiliary control input vector.

From Eqs. (12) and (38), the following is obtained

$$\ddot{\mathbf{q}}_C - \ddot{\mathbf{q}}_E = \boldsymbol{\eta}\,. \tag{39}$$

Second, the auxiliary control input vector $\boldsymbol{\eta} \equiv [\eta_1 \quad \eta_2 \quad \eta_3]^T$ is chosen as a control law.

$$\boldsymbol{\eta} = \mathbf{G}^{-1}\{\mathbf{QS} + \mathbf{Psign(S)} + \boldsymbol{\Delta}_1\} \tag{40}$$

where $\mathbb{N}_1 = \begin{bmatrix} \dot{\omega}_C(e_5 + D) + 2\omega_C\dot{e}_5 + \omega_C^2 e_4 + k_4\dot{e}_4 \\ -\dot{\omega}_C e_4 - 2\omega_C\dot{e}_4 + \omega_C^2(e_5 + D) + k_5\dot{e}_5 \\ k_6\dot{e}_6 \end{bmatrix}$

$\mathbf{P} = diag(P_4, P_5, P_6)$ and $\mathbf{Q} = diag(Q_4, Q_5, Q_6)$ are diagonal positive definite matrices.

Theorem 3.2: For the dynamic model of OMP Eq. (12) with a friction torque disturbance vector, if the control laws in Eqs. (38) and (40) are applied, a sliding surface vector $\mathbf{S}$ and a posture error vector $\mathbf{e}$ converge to zero asymptotically as $t \to \infty$.

Proof: The Lyapunov function candidate is chosen as

$$V_2 = \frac{1}{2}\mathbf{S}^{\mathrm{T}}\mathbf{S}\,. \tag{41}$$

With Eqs. (35), (36), (39) and (40), the first order derivative of $\mathbf{S}$ is obtained as

$$\begin{aligned}\dot{\mathbf{S}} &= \begin{bmatrix} \dot{S}_4 \\ \dot{S}_5 \\ \dot{S}_6 \end{bmatrix} = \begin{bmatrix} \ddot{e}_4 + k_4\dot{e}_4 \\ \ddot{e}_5 + k_5\dot{e}_5 \\ \ddot{e}_6 + k_6\dot{e}_6 \end{bmatrix} = \mathbf{G}[\ddot{\mathbf{q}}_E - \ddot{\mathbf{q}}_C] + \boldsymbol{\Delta}_1 \\ &= -\mathbf{G}\boldsymbol{\eta} + \boldsymbol{\Delta}_1 = -\mathbf{QS} - \mathbf{Psign(S)}\end{aligned}\,. \tag{42}$$

The first order derivative of V_2 is derived into

$$\begin{aligned}\dot{V}_2 &= \mathbf{S}^{\mathrm{T}}\dot{\mathbf{S}} = \mathbf{S}^{\mathrm{T}}[-\mathbf{QS} - \mathbf{Psign(S)}] \\ &= -\sum_{i=4}^{6}\left[Q_i S_i^2 + P_i|S_i|\right] \le 0\end{aligned}\,. \tag{43}$$

If $Q_i \ge 0$ and $P_i \ge 0$ ($i = 4, 5, 6$), $\dot{V}_2$ is negative semi-definite. By Barbalat's lemma [16], $\mathbf{S} \to 0$ as $t \to \infty$. Because there exists the control law $\boldsymbol{\eta}$ stabilizing the sliding surface vector in Eq. (37), the tracking error vector $\mathbf{e}$ converges to zero as $t \to \infty$.

In order to eliminate the chattering phenomenon, the sig-

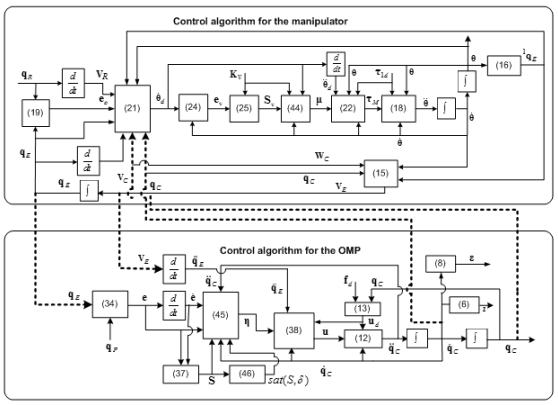

Fig. 5. Block diagram for the proposed control system.

num function $sign(\cdot)$ is replaced by a saturation function $sat(\cdot)$ [17]. The control laws in Eqs. (26) and (40) can be re-expressed as follows:

$$\boldsymbol{\mu} = -\mathbf{Q}_v\mathbf{S}_v - \mathbf{P}_v\,\mathbf{sat}(\mathbf{S}_v,\delta) - \mathbf{K}_v(\dot{\boldsymbol{\theta}} - \dot{\boldsymbol{\theta}}_d) \tag{44}$$

$$\boldsymbol{\eta} = \mathbf{G}^{-1}\left\{\mathbf{QS} + \mathbf{Psat}(\mathbf{S},\delta) + \boldsymbol{\Delta}_1\right\} \tag{45}$$

where the saturation function $sat(\cdot)$ is defined as:

$$sat(S_o,\delta) = \begin{cases} S_o/\delta & if\ |S_o/\delta| \le 1 \\ sign(S_o/\delta) & otherwise \end{cases} \tag{46}$$

where S_o is any general chosen sliding surface, δ is a boundary layer thickness.

The block diagram for the proposed controller of the OMMS is shown in Fig. 5. A decentralized control strategy is applied to the OMMS that includes two controllers for the manipulator and the omnidirectional mobile platform. The position vector $\mathbf{q}_C$ and the velocity vector $\mathbf{V}_C$ as the outputs of the OMP are fed as inputs of the controller of the manipulator. The position vector $\mathbf{q}_E$ and the velocity vector $\mathbf{V}_E$ as the outputs of the manipulator are fed as the inputs of the controller of the OMP.

4. Error measurement and hardware

4.1 Tracking errors using touch sensor

A touch sensor is used to measure tracking errors between the end-effector and reference point as shown in Fig. 6. The touch sensor consists of two rollers and two potentiometers: one is a rotary potentiometer, and another is a linear potentiometer. Two rollers are mounted on a bar that can rotate around the pivot of a rotary potentiometer. This potentiometer is mounted on another bar that can slide along the third link, and the displacement can be measured by a linear potentiometer. Tracking errors detected using the touch sensor are as follows [10-12, 15]:

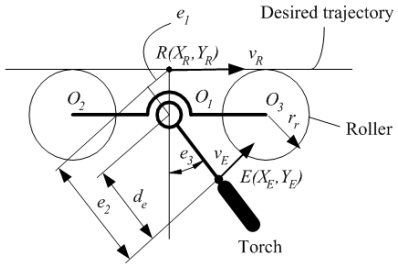

Fig. 6. Configuration of measuring tracking errors using touch sensor.

$$\begin{aligned} e_1 &= -r_r \sin e_3, \\ e_2 &= d_e + r_r \cos e_3, \\ e_3 &= \angle(O_1E, O_1O_3) - \frac{\pi}{2} \end{aligned} \tag{47}$$

where r_r is the radius of the roller, d_e is the length which is measured by the linear potentiometer, and e_3 is the angle which is measured by the rotary potentiometer O_2O_3

This method is also applied for a curve line if the distance of O_2O_3 is small enough, and the curved radius of a desired trajectory is large enough. The method is used to determine errors for designing a controller.

4.2 Posture errors

The posture errors e_4, e_5 and e_6 in Fig. 4 can be calculated as follows [10-12]:

$$\begin{aligned} e_4 &= x_E - x_P = L_1\cos\theta_1 + L_2\cos(\theta_1+\theta_2) \\ &\quad + L_3\cos(\theta_1+\theta_2+\theta_3) \\ e_5 &= y_E - y_P = L_1\sin\theta_1 + L_2\sin(\theta_1+\theta_2) \\ &\quad + L_3\sin(\theta_1+\theta_2+\theta_3) - D \\ e_6 &= \phi_E - \frac{\pi}{2} = (\theta_1+\theta_2+\theta_3) - \frac{\pi}{2} \end{aligned} \tag{48}$$

where $(x_E \quad y_E \quad \phi_E)$ is denoted as the coordinates with respect to the moving coordinate frame of the point E, $(x_P \quad y_P \quad \phi_P)$ is the coordinates with respect to the moving coordinate frame of the point P, and the joint angles θ_1, θ_2 and θ_3 can be measured by the rotary potentiometers which are mounted at each joint of the manipulator.

4.3 Hardware

A prototype of the experimental OMMS with six degrees-of-freedom (DOFs) is shown in Fig. 7(a). The OMMS is considered as two subsystems such as a manipulator and an OMP. The manipulator has three DOFs, each driven by a DC encoder motor (50.8 W/24 V) with gear ratio 144:1. The touch for measuring the tracking errors is mounted on the third link. The rotary potentiometers for measuring the joint angles are mounted at each joint. The mobile platform has three omnidirectional wheels that are driven by 3 DC encoder motors (39.7

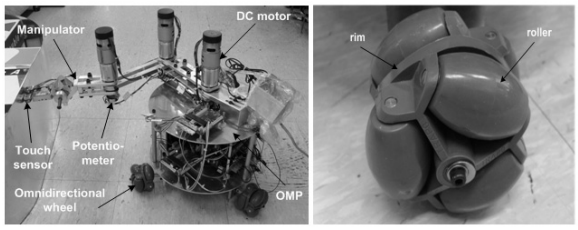

(a) Prototype (b) Omnidirectional wheel

Fig. 7. Experimental OMMS.

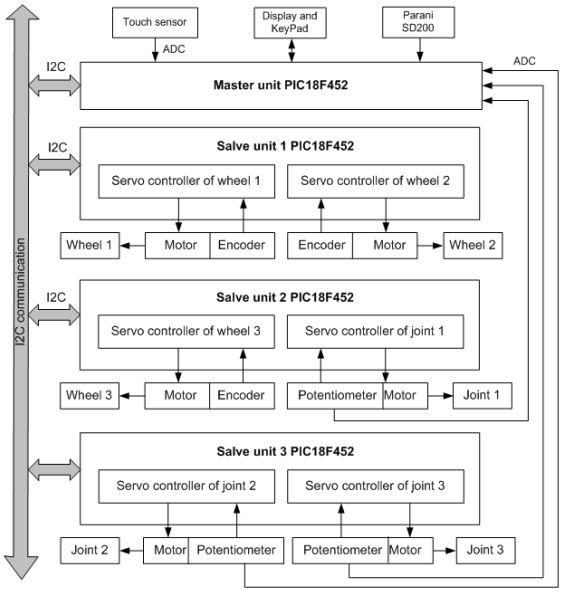

Fig. 8. Control architecture of hardware system of the OMMS.

W/24 V) with the gear ratio 71:1. The omnidirectional wheel used for this paper is shown in Fig. 7(b).

The omnidirectional wheel in Fig. 7(b) is an assembly that provides both constrained and unconstrained motions when turning. It has six rollers aligned around its rim so that it can roll freely orthogonally to its driving direction. Because three wheels are mounted on a platform, their constrained and unconstrained motions can be combined to provide omnidirectionality. An omnidirectional mobile platform can simultaneously perform independent translation and rotation. With the above capabilities, the omnidirectional mobile platform makes the omnidirectional mobile manipulator more efficient and dexterous than the regular mobile manipulator.

4.4 Control system

A control system is developed based on PIC18F452 type of microcontrollers which are operated with the clock frequency 40MHz. A hardware configuration of the proposed control system using seven PIC18F452's is shown in Fig. 8.

One PIC18F452 is used as the master unit, and other PIC18F452's are used as slave units. The design control algorithms are embedded into PIC18F452 for controlling the DC motors at the joints of the manipulator and the three wheels of the OMP. The master unit functions as the main controller, that is, to receive the tracking error vector of the end-effector using the touch sensor and the angles of joints of the manipulator using potentiometers and, in turn, to send the commands to the slave controllers via I2C communication, respectively. The master unit can be used to interface other devices such as display and keypad devices or personal computer via RS-232 communication for remote control through a Parani SD200 blue tooth. The slave unit integrates PIC18F452 with LMD18200 motor drivers for the DC motor control. The servo controller of the slave unit can perform a complete servo operation with a closed loop feedback control using an encoder for velocity control of three wheels and using potentiometer for position control of each joint. The sampling time of the proposed control system is about 10 ms.

Table 1. Numerical parameter values of the DC motor and the OMMS.

Parameters	Values	Units
R_a	20.5	[Ω]
k_e	7.2x10-2	[Nm/A]
k_t	7.2x10-2	[Nm/A]
u	24	[V]
τ	3.1	[kg.cm]
n	71	[rpm]
r	0.04	[m]
α	0.087	$[N/V]$
β	11.4	$[kg/s]$
r	0.04	$[m]$
L	0.18	$[m]$
$L_1 = L_2 = L_3 = L_o$	0.18	$[m]$
$m_1 = m_2 = m_3$	0.95	$[kg]$
m	9.5	$[kg]$
I	0.19	$[kgm^2]$
g	9.8	$[m/s^2]$

5. Simulation and experiment results

5.1 Simulation results

To verify the effectiveness of the proposed controller, simulations have been done for the OMMS to track a desired trajectory. The numerical values of parameters, the numerical parameter values, and the initial values of the DC motor and the OMMS for simulation and experiment are given in Table 1 and Table 2. Fig. 9 shows the desired trajectory with a straight line of $l_1 = 0.3\ m$, a curved line of $(r_1 = 0.3m, 90^0)$, a straight line of $l_2 = 0.3\ m$, a curved line of $(r_2 = 0.3m, 180^0)$, and a straight line of $l_3 = 0.3\ m$. The desired velocity of the end-effector is $v_R = 0.01\ m/s$. The sampling time of control system is about 10 ms.

The designed parameters of the proposed controller are as

Table 2. The initial values for simulation.

Parameters	Values	Units
X_R	0.4	$[m]$
Y_R	0.4	$[m]$
Φ_R	0	[deg]
X_E	0.395	$[m]$
Y_E	0.395	$[m]$
Φ_E	5	[deg]
v_R	0.01	$[m/s]$

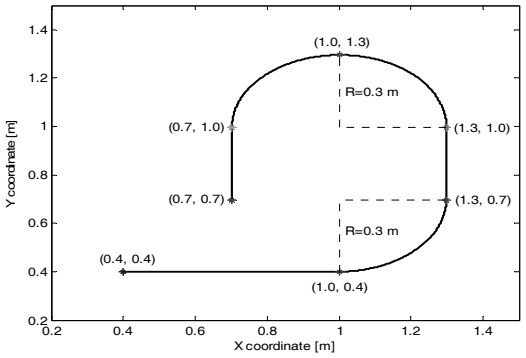

Fig. 9. Control architecture of hardware system of the OMMS.

follows: $k_1 = 1.7\ s^{-1}$, $k_2 = 1.7\ s^{-1}$, $k_3 = 1.7\ s^{-1}$, $k_{v1} = 0.2\ s^{-1}$, $k_{v2} = 0.2\ s^{-1}$, $k_{v3} = 0.2 s^{-1}$, $k_4 = 0.4 s^{-1}$, $k_5 = 1.5 s^{-1}$, $k_6 = 0.4 s^{-1}$, $P_{v4} = 0.3 s^{-1}$, $P_{v5} = 0.3 s^{-1}$, $P_{v6} = 0.3 s^{-1}$, $P_4 = 0.2 s^{-1}$, $P_5 = 0.2 s^{-1}$, $P_6 = 0.2 s^{-1}$, $Q_{v4} = 15 s^{-1}$, $Q_{v5} = 15 s^{-1}$, $Q_{v6} = 15 s^{-1}$, $Q_4 = 20 s^{-1}$, $Q_5 = 20 s^{-1}$, $Q_6 = 20 s^{-1}$ and $\delta = 0.1$. The maximum magnitudes of friction torque disturbances are assumed as $f_{Mi} = 4\ N$ and $f_{Ai} = 3\ N$ $(i = 1, 2, 3)$. The periodic external disturbances vector to influence the manipulator is assumed to be $\tau_{1d} = [0.1\sin(2t)\ \ 0.1\sin(2t)\ \ 0.1\cos(2t)]^T$.

The simulation results for trajectory tracking of the manipulator are shown in Figs. 10-29. Figs. 10-12 show the force disturbance vector that is exerted on the OMP for the full time. f_{1d}, f_{2d} and f_{3d} change in time within $\pm 8\ N$, $\pm 8\ N$ and $\pm 2.16\ Nm$, respectively. Figs. 13 and 14 show a control input torque vector $\boldsymbol{\tau}_M$ and an auxiliary control input vector $\boldsymbol{\mu}$ of the manipulator. They change at the beginning time and converge to constant values within $\pm 2\ Nm$ and $\pm 0.01\ rad/s^2$, respectively. Figs. 15 and 16 show a control input voltage vector $\mathbf{u}$ and an auxiliary control input vector $\boldsymbol{\eta}$ of the OMP, respectively. They are bounded, and its average value converges to constant values within $\pm 24\ V$ and $\pm 0.2\ m/s^2$, respectively. The tracking error vectors are shown in Figs. 17-18 at the beginning time and for the full time. They show that the kinematic controller of the manipulator makes the tracking errors e_1, e_2, e_3 converge to zero asymptotically after about 4 seconds for tracking the desired trajectory. The integral sliding surface vector $\mathbf{S}_v$ approaches zero from 4 seconds as shown in Fig. 19. So the angular velocity error vector $\mathbf{e}_v$ also goes to zero from 4 seconds as shown in Fig. 20 and it maintains zero values for the full time as shown in

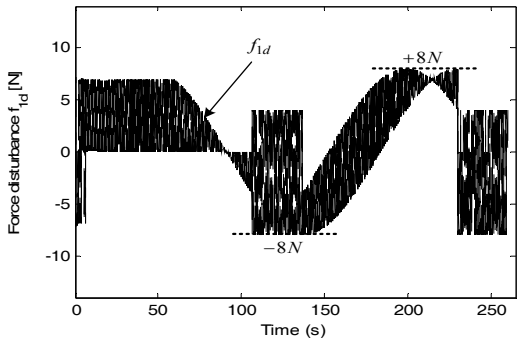

Fig. 10. Force disturbance f_{1d}.

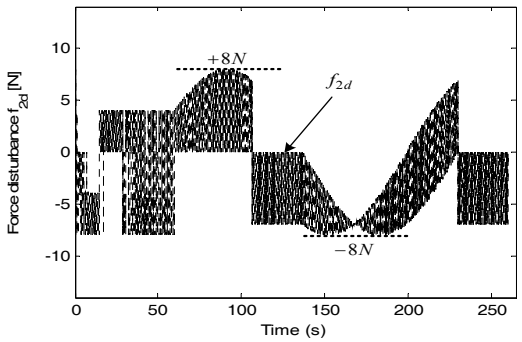

Fig. 11. Configuration Force disturbance f_{2d}.

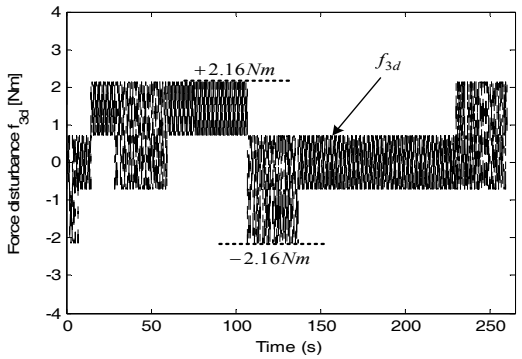

Fig. 12. Force disturbance f_{3d}.

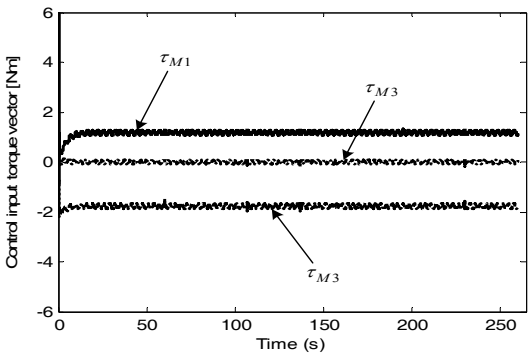

Fig. 13. Control input torque vector $\boldsymbol{\tau}_M$ of the manipulator.

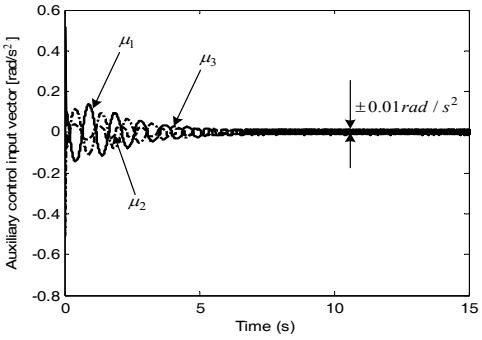

Fig. 14. Auxiliary control input vector $\boldsymbol{\mu}$ of the manipulator.

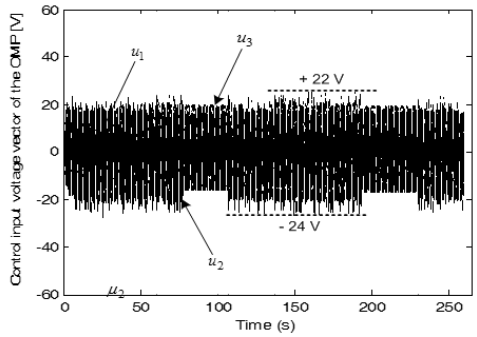

Fig. 15. Control input voltage vector $\mathbf{u}$ of the OMP.

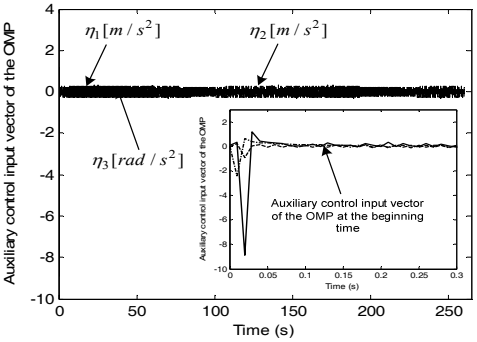

Fig. 16. Auxiliary control input vector $\boldsymbol{\eta}$ of the OMP.

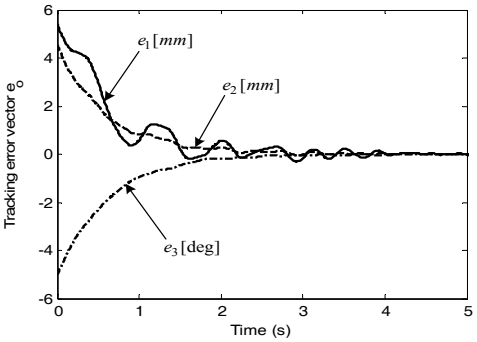

Fig. 17. Tracking error vector $\mathbf{e}_o$ at the beginning time.

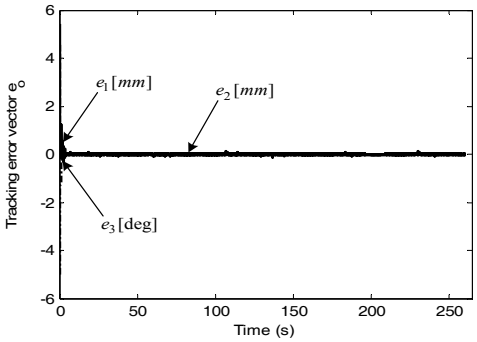

Fig. 18. Tracking error vector $\mathbf{e}_o$ for the full time.

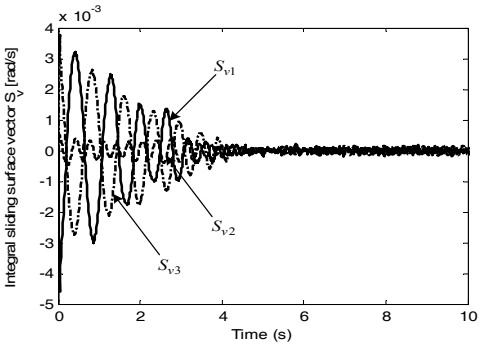

Fig. 19. Integral sliding surface vector $\mathbf{S}_v$ at the beginning time.

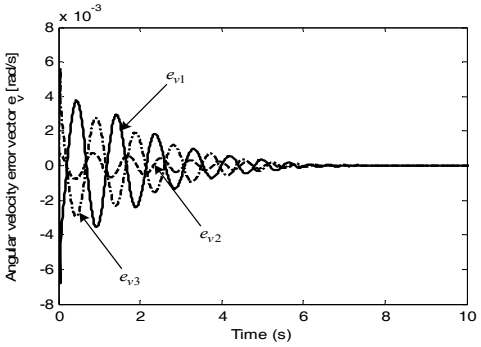

Fig. 20. Angular velocity error vector $\mathbf{e}_v$ at the beginning time.

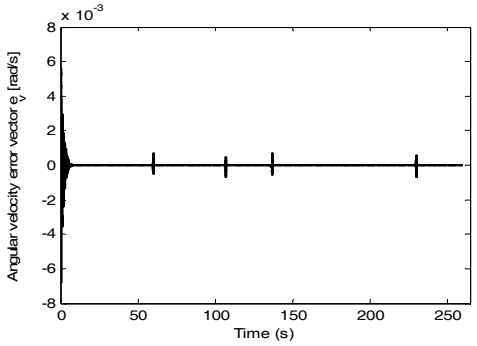

Fig. 21. Angular velocity error vector $\mathbf{e}_v$ for the full time.

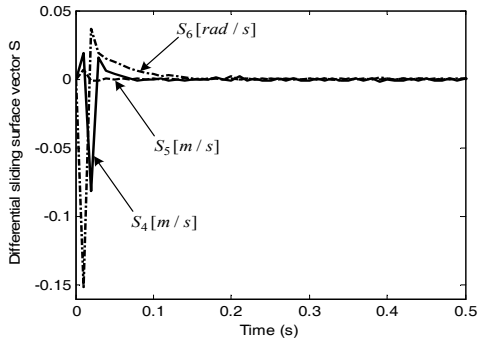

Fig. 22. Differential sliding surface vector **S** at the beginning time.

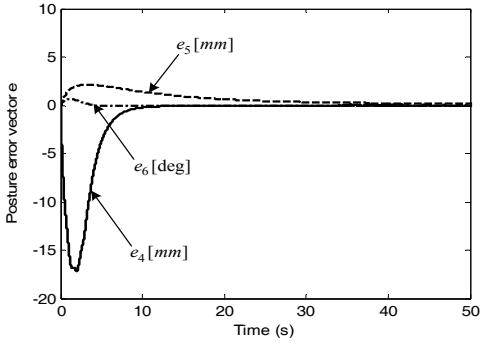

Fig. 23. Posture error vector **e** at the beginning time.

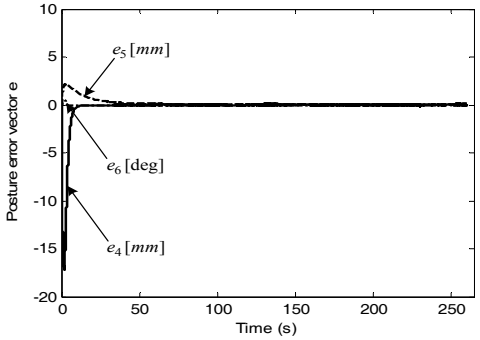

Fig. 24. Posture error vector **e** for the full time.

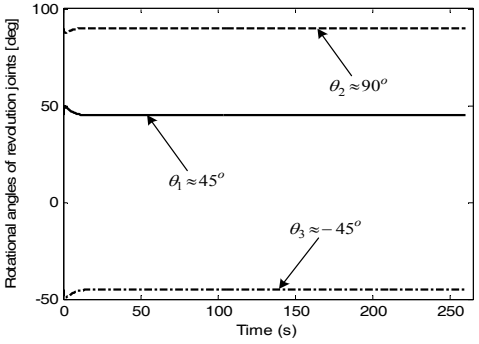

Fig. 25. Rotational angles of revolution joints.

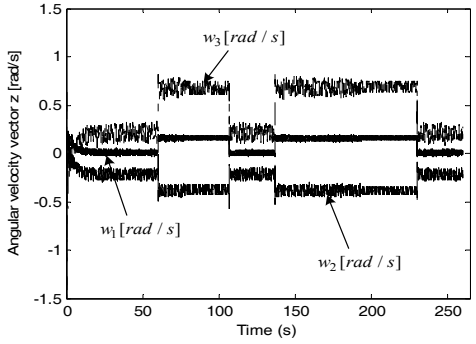

Fig. 26. Angular velocities of three wheels.

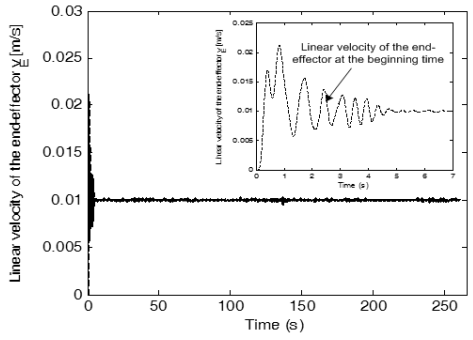

Fig. 27. Linear velocity v_E of the end-effector.

Fig. 21. The differential sliding surface vector **S** approaches zero very quickly from 0.2 second as shown in Fig. 22. So the posture error vector **e** also goes to zero as shown in Fig. 23 and it maintains zero values for the full time as shown in Fig. 24. They show that the tracking errors e_4, e_5, e_6 converge to zero more slowly than e_1, e_2, e_3 because the end-effector first approaches the reference point as soon as possible and then the OMP allows the manipulator to move to the desired posture without its singularity. Rotational angles of revolution joints are shown in Fig. 25. After 12 seconds, θ_1, θ_2 and θ_3 go to the desired values of $\theta_1 = 45^o$, $\theta_2 = 90^o$ and $\theta_3 = -45^o$. This means that the manipulator approaches the desired posture. The angular velocities of the three wheels are shown in Fig. 26. It shows that the angular velocity values are $\omega_1 = 0$, $\omega_2 = -\omega_3 = -0.21\ rad/s$ for tracking the straight lines; $\omega_1 = 0.154\ rad/s$, $\omega_2 = -0.382\ rad/s$, $\omega_3 = 0.679\ rad/s$ and $|\omega_3| > |\omega_2|$ for left turning in tracking the arc lines. The linear velocity of the end-effector is about $0.01\ m/s$, as desired, from 5 seconds, as shown in Fig. 27. Figs. 28 and 29 show the movement of the OMMS along the desired trajectory at the beginning time and for the full time of 260.4 seconds. The above simulation results show that the proposed tracking controller has a good trajectory tracking performance under disturbance and friction.

5.2 Experiment results

The simulation and experimental results are shown in Figs. 30-38. Figs. 29-32 show the simulation and experimental tracking errors for the full time, 260.4 seconds. It shows that

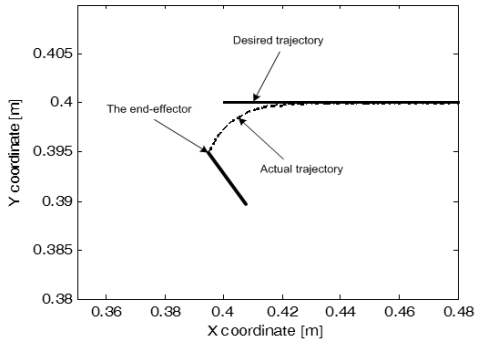

Fig. 28. Movement of the OMMS at the beginning time.

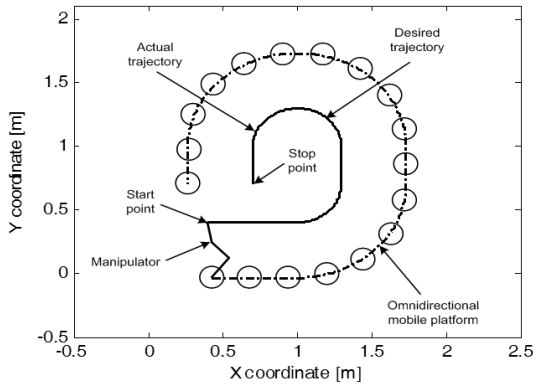

Fig. 29. Movement of the OMMS for the full time.

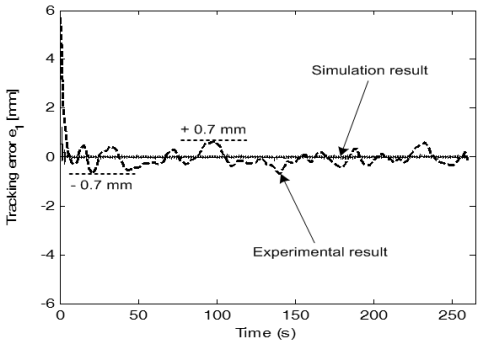

Fig. 30. Simulation and experimental results of tracking error e_1.

the experimental results of the tracking errors e_1, e_2 and e_3 are bounded along the simulation results within $\pm 0.7mm$, $\pm 0.8mm$ and ± 2.3deg, respectively. Figs. 33-35 show the simulation and experimental results for the posture error vector for full time 260.4 seconds. It shows that the experiment results of the posture errors e_4, e_5 and e_6 are bounded along the simulation results within $\pm 1.3mm$, $\pm 0.6mm$ and ± 1.4deg, respectively. Figs. 36-38 also show the simulation and experimental results for rotational angles of revolution joints. The experiment results are bounded within ± 2.1deg, ± 1.7deg and ± 1.8deg along the simulation results with respects to the desired values $\theta_1 = 45^o$, $\theta_2 = 90^o$ and $\theta_3 = -45^o$, respectively. It means that the manipulator keeps the desired posture without singularity during the operation's process. The simulation and experimental results show the effectiveness and the applicability of the OMMS to practical fields.

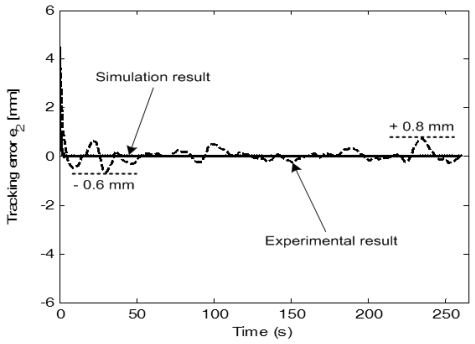

Fig. 31. Simulation and experimental results of tracking error e_2.

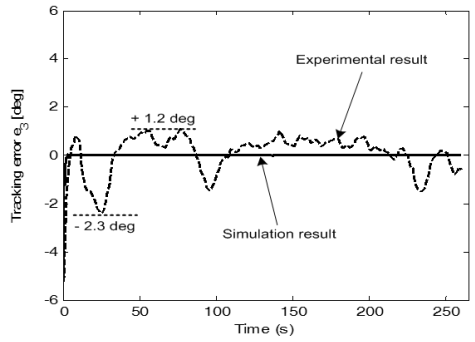

Fig. 32. Simulation and experimental results of tracking error e_3.

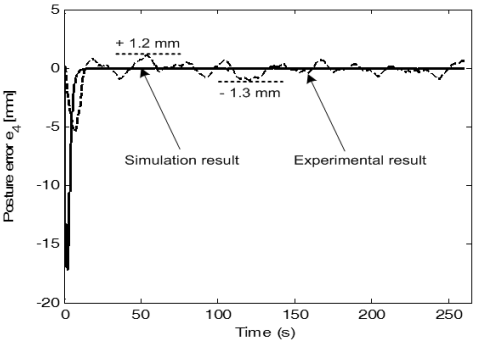

Fig. 33. Simulation and experimental results of posture error e_4.

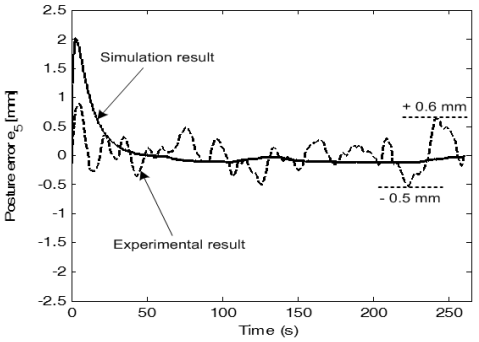

Fig. 34. Simulation and experimental results of posture error e_5.

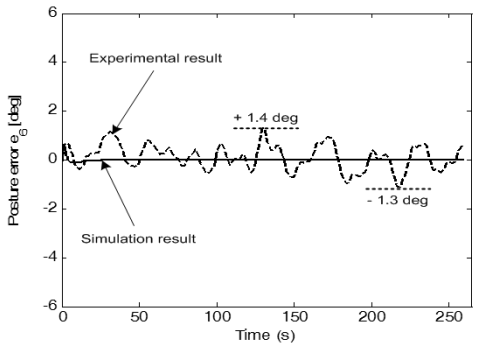

Fig. 35. Simulation and experimental results of posture error e_6.

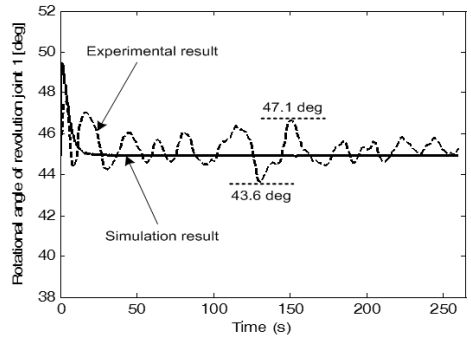

Fig. 36. Simulation and experimental results of rotational angle θ_1 of revolution joint 1.

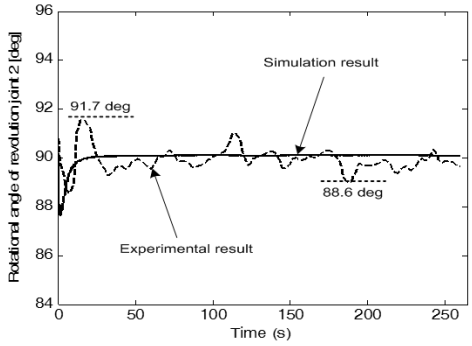

Fig. 37. Simulation and experimental results of rotational angle θ_2 of revolution joint 2.

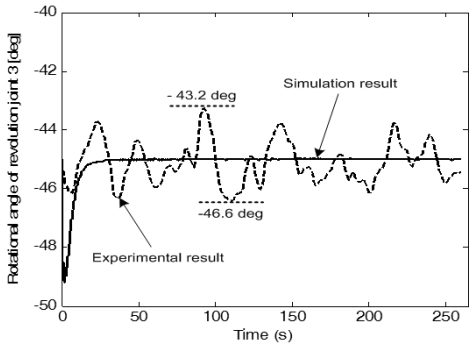

Fig. 38. Simulation and experimental results of rotational angle θ_3 of revolution joint 3.

6. Conclusions

This paper proposes an OMMS for trajectory tracking of the manipulator with trajectory with constant velocity. The OMMS is divided into two subsystems such as a manipulator and an OMP. A decentralized control strategy is applied for this system using sliding mode robust control technique. The kinematic controller (KC) combined with the integral sliding mode controller (ISMC) and the differential sliding mode controller (DSMC) are designed to control the manipulator and the OMP, respectively. The control laws are obtained based on Lyapunov stability theory and make the tracking error vectors go to zero asymptotically. The experimental results are bounded within some values along the simulation results. The simulation and experiment results are presented to illustrate the effectiveness and the applicability to the practical fields of the proposed controller of the OMMS.

References

[1] F. G. Pin and S. M. Killough, A new familly of omnidirectional and holonomic wheeled platforms for mobile robots, *IEEE Trans. on Robotics and Automation*, 10 (4) (1994) 490-489.

[2] A. Betourne and G. Campion, Dynamic modelling and control design of a class of omnidirectional mobile robots, *Proceedings of the 1996 IEEE Iternational Conference on Robottics and Automation*, Minnesota (1996) 2810-2815.

[3] K. Watanabe, Y. Shiraishi, S. G. Tzafestas, J. Tang and T. Fukuda, Feedback control of an omnidirectional autonomous platform for mobile service robots, *J. Intell. Robot. Syst.*, 22 (1998) 315-330.

[4] H. C. Huang and C. C. Tsai, Adaptive robust control of an omnidirectional mobile platform for autonomous service robots in polar coordinates, *J. Intell. Robot. Syst.*, 51 (4) (2008) 439-460.

[5] H. C. Huang and C. C. Tsai, FPGA Implementation of an embedded robust adaptive controller for autonomous omnidirectional mobile platform, *IEEE Trans. on Industrial Electronics*, 56 (5) (2009) 1604-1616.

[6] K. Watanabe, K. Sato, K. Izumi and Y. Kunitake, Analysis and control for an omnidirectional mobile manipulator, *J. Intell. Robot. Syst.,* 27 (2000) 3-20.

[7] D. Xu, D. Zhao, J. Yi and X. Tan, Trajectory tracking control of omnidirectional wheeled mobile manipulators robust neural network-based sliding mode approach, *IEEE Trans. on Systems, Man, and Cybernetics*, 39 (3) (2009) 788-799.

[8] T. K. Nagy, R. D'Andrea and P. Ganuly, Near-optimal dynamic trajectory generation and control of an omnidirectional vehicle, *Robotics and Autonomous Systems*, 47 (1) (2004) 47-64.

[9] R. L. Williams II, B. E. Carter, P. Gallina and G. Rosati, Dynamic model with slip for wheeled omnidirectional robots, *IEEE Trans. on Robotics and Automation*, 18 (3) (2002) 285-293.

[10] N. Hung, D. W. Kim, H. K. Kim and S. B. Kim, Tracking

controller design of omnidirectional mobile manipulator system, *ICROS-SICE International Joint Conference*, Fukuoka (2009) 539-544.

[11] T. T. Phan, T. L. Chung, M. D. Ngo, H. K. Kim and S. B. Kim, Decentralized control design for welding mobile manipulator, *International Journal of KSME*, 19 (3) (2005) 756-767.

[12] M. D. Ngo, N. T. Phuong, V. H. Duy, H. K. Kim and S. B. Kim, Control of two wheeled welding mobile manipulator, *International Journal of Advanced Robotics System*, 4 (3) (2007) 293-302.

[13] F. L. Lewis, C. T. Abdallah and D. M. Dawson, Control of mabot manipulator, *Prentice Hall International Edition* (1993).

[14] F. L. Lewis, C. T. Abdallah and D. M. Dawson, Control of robot manipulator, *Prentice Hall International Edition* (1993).

[15] T. L. Chung, H. T. Bui, T. T. Nguyen and S. B. Kim, Sliding mode control of two-wheeled welding mobile robot for tracking smooth curved welding path, *International Journal of KSME*, 18 (7) (2004) 1094-1106.

[16] J. J. E. Slotine and W. Li, Applied nonlinear control, *Prentice-Hall International, Inc*. (1991).

[17] H. K. Khalil, Nonlinear systems, *Prentice-Hall International, Inc.*, (2002).

[18] Y. M. Sam, J. H. S. Osman and M. R. A. Ghani, *A class of proportional-integral sliding mode control with application to active suspension system*, Systems & Control Letters, 51 (3-4) (2004) 217-223.

[19] H. Zhang, Y. Shi, A. S. Mehr, Robust $\mathcal{H}_\infty$ PID control for multivariable networked control systems with disturbance/noise attenuation, *International Journal of Robust and Nonlinear Control*, DOI: 10.1002/rnc.1688 (2011).

Appendix

From Fig. 2(b) using Lagrange formula, the parameters of Eq. (18) can be obtained as follows:

$$M_{11} = (m_1 + 5m_2 + 9m_3)\frac{L_o^2}{4} + (\frac{m_2}{2} + m_3)L_o^2\cos\theta_2 + m_3L_o^2\cos(\theta_2+\theta_3) + m_3L_o^2\cos\theta_3 \ ,$$

$$M_{12} = (\frac{m_2}{2} + m_3)L_o^2\cos\theta_2 + \frac{m_3}{2}L_o^2\cos(\theta_2+\theta_3) + m_3L_o^2\cos\theta_3 \ ,$$

$$M_{13} = \frac{m_3}{2}L_o^2\cos(\theta_2+\theta_3) + \frac{m_3}{2}L_o^2\cos\theta_3 \ ,$$

$$M_{21} = (\frac{m_2}{2} + m_3)L_o^2\cos\theta_2 + \frac{m_3}{2}L_o^2\cos(\theta_2+\theta_3) + m_3L_o^2\cos\theta_3 \ ,$$

$$M_{22} = (\frac{m_2}{4} + m_3)L_o^2 + \frac{m_3}{4}L_o^2 + m_3L_o^2\cos\theta_3 \ ,$$

$$M_{23} = \frac{m_3}{2}L_o^2\cos\theta_3 \ ,$$

$$M_{31} = \frac{m_3}{2}L_o^2\cos(\theta_2+\theta_3) + \frac{m_3}{2}L_o^2\cos\theta_3 \ ,$$

$$M_{32} = \frac{m_3}{2}L_o^2\cos\theta_3 \ ,$$

$$M_{33} = \frac{m_3}{4}L_o^2 \ ,$$

$$V_{11} = -(\frac{m_2}{2} + m_3)L_o^2(2\dot\theta_1\dot\theta_2 + \dot\theta_2^2)\sin\theta_2 - \frac{m_3}{2}L_o^2(2\dot\theta_1\dot\theta_2 + 2\dot\theta_1\dot\theta_3 + 2\dot\theta_2\dot\theta_3 + \dot\theta_2^2 + \dot\theta_3^2)\sin(\theta_2+\theta_3) - \frac{m_3}{2}L_o^2(2\dot\theta_1\dot\theta_3 + 2\dot\theta_2\dot\theta_3 + \dot\theta_3^2)\sin\theta_3$$

$$V_{21} = -(\frac{m_2}{2} + m_3)L_o^2\dot\theta_1\dot\theta_2\sin\theta_2 - \frac{m_3}{2}L_o^2(\dot\theta_1\dot\theta_2 + \dot\theta_1\dot\theta_3)\sin(\theta_2+\theta_3) - \frac{m_3}{2}L_o^2(2\dot\theta_1\dot\theta_3 + 2\dot\theta_2\dot\theta_3 + \dot\theta_3^2)\sin\theta_3 \ ,$$

$$V_{31} = -\frac{m_3}{2}L_o^2(\dot\theta_1\dot\theta_2 + \dot\theta_1\dot\theta_3)\sin(\theta_2+\theta_3) - \frac{m_3}{2}L_o^2(\dot\theta_1\dot\theta_3 + \dot\theta_2\dot\theta_3)\sin\theta_3 + \frac{m_3}{2}L_o^2(\dot\theta_1^2 + \dot\theta_1\dot\theta_2 + \dot\theta_1\dot\theta_3)\sin(\theta_2+\theta_3) + \frac{m_3}{2}L_o^2(\dot\theta_1^2 + \dot\theta_2^2 + 2\dot\theta_1\dot\theta_2 + \dot\theta_1\dot\theta_3 + \dot\theta_2\dot\theta_3)\sin\theta_3 \ ,$$

$$G_{11} = (\frac{m_1}{2} + m_2 + m_3)gL_o\cos\theta_1 + (\frac{m_2}{2} + m_3)gL_o\cos(\theta_1+\theta_2) + \frac{m_3}{2}gL_o\cos(\theta_1+\theta_2+\theta_3) \ ,$$

$$G_{21} = (\frac{m_2}{2} + m_3)gL_o\cos(\theta_1+\theta_2) + \frac{m_3}{2}gL_o\cos(\theta_1+\theta_2+\theta_3) \ ,$$

$$G_{31} = \frac{m_3}{2}gL_o\cos(\theta_1+\theta_2+\theta_3) \ ,$$

$$\boldsymbol{\tau}_{1d} = [\tau_{1m}\sin(2t) \ \ \tau_{2m}\sin(2t) \ \ \tau_{2m}\cos(2t)]^T \ .$$

where m_1, m_2, m_3 are the masses of links and $L_1 = L_2 = L_3 = L_o$, τ_{1m}, τ_{2m}, and τ_{3m} are magnitudes of disturbance torques exerted on three-linked manipulator.

Tuan Dinh Viet was born in Vietnam on July 14, 1972. He received a B.S. degree in the Faculty of Computer Science, Hochiminh City Open University, Vietnam in 1997. He received a B.S. degree in the Faculty of Information Technology, College of Engineering, University of Danang, Vietnam in 2008. He is currently a Ph.D. student in the Dept. of Mechanical Engineering, Pukyong National University, Busan, Korea. His fields of interests are computer science, robust control and mobile robot control.

Phuc Thinh Doan was born in Vietnam on January 31, 1985. He received a B.S. degree in the Dept. of Mechanical Engineering, Hochiminh City University of Technology, Vietnam in 4/2007. He then received an M.S. degree in the Dept. of Mechanical Engineering, Pukyong National University, Busan, Korea in 2/2011. He is currently a Ph.D. student in the Dept. of Mechanical Engineering, Pukyong National University, Busan, Korea. His fields of interests are robotic, power electric, motion control and mobile robot control.

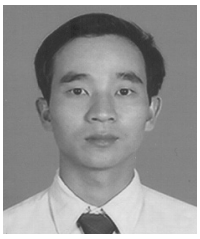

Nguyen Hung was born in Vietnam on December 01, 1977. He received B.S. and M.S. degrees in the Faculty of Electrical and Electronics Engineering, Hochiminh City University of Technology, Vietnam in 2000 and 2004. He then received his Ph.D. in the Dept. of Mechanical Engineering, Pukyong National University, Busan, Korea in 2/2010. Since then, he has been a lecturer of Faculty of Mechanical – Electrical – Electronic, University of Technology, Hochiminh City, Vietnam. His fields of interests are robust control and mobile robot control.

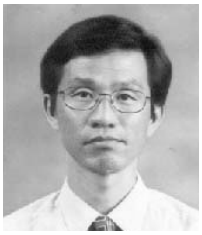

Hak Kyeong Kim was born in Korea on November 11, 1958. He received B.S. and M.S. degrees in the Dept. of Mechanical Engineering from Pusan National University, Korea in 1983 and 1985. He received his Ph.D. degree from the Dept. of Mechatronics Engineering, Pukyong National University, Busan, Korea in February, 2002. His fields of interest are robust control, biomechanical control, mobile robot control, and image processing control.

Sang Bong Kim was born in Korea on August 6, 1955. He received B.S. and M.S. degrees from the National Fisheries University of Pusan, Korea in 1978 and 1980. He received his Ph.D. from Tokyo Institute of Technology, Japan in 1988. Since then, he has been a Professor of the Dept. of Mechanical Engineering, Pukyong National University, Busan, Korea. His research has been on robust control, biomechanical control, and mobile robot control.